Mon. Not. R. astr. Soc. (1987) **227,** 1013–1020

IRAS observations of southern molecular clouds

T. B. H. Kuiper *Jet Propulsion Laboratory, 169-506, California Institute of Technology, Pasadena, California 91109, USA*

J. B. Whiteoak *Division of Radiophysics, CSIRO, PO Box 76, Epping, NSW 2121, Australia*

J. W. Fowler and W. Rice *Infrared Processing and Analysis Center, California Institute of Technology, 100-22, Pasadena, California 91125, USA*

Accepted 1987 March 25. Received 1987 March 19; in original form 1987 January 2

Summary. A report is given of a project to use *IRAS* Band 3 (60 μm) and Band 4 (100 μm) observations to investigate the far-infrared properties of southern galactic molecular clouds. A method by which dust temperature and total gas column density can be estimated is presented. Results are tabulated for 65 prominent southern far-infrared sources. The dust temperatures are closely grouped between 30 and 50 K, while the column densities range between 2×10^{20} and 10^{22} cm^{-2}. Maps of dust temperature and gas column density have been generated for two fields containing far-infrared sources to illustrate the effectiveness of this form of presentation.

1 Introduction

Radio line surveys of southern molecular clouds have generally been based on catalogues of visible nebulae and radio continuum sources (e.g. Whiteoak 1983). Thus sites of star formation without such indicators may have been missed by such surveys.

A more complete identification of molecular clouds is possible by observation of the dust associated with the molecular clouds. Considerable research has been carried out on the principal heating sources of the interstellar dust of our Galaxy. In an interpretation of the IR and submillimetre emission observed towards the inner galactic regions, Cox, Krugel & Mezger (1986) proposed contributions from several dust components with specific temperature ranges. Two are associated with molecular clouds. Cool dust is found in quiescent molecular clouds and a warmer component is associated with ionized gas or shells surrounding early-type stars. The total temperature range for these dust components is 14 to 40 K. The emission associated with such temperatures is concentrated between the wavelengths 20 and 1000 μm. On this basis the observations in Band 3 (60 μm) and Band 4 (100 μm) of the *IRAS* far-IR sky survey should be particularly useful for identification of the dust associated with molecular clouds. Moreover, the

ratios of the brightnesses in the bands can provide estimates of the dust temperature and gas column density within the clouds.

We have begun a project to identify and study southern molecular clouds present in the *IRAS* survey. Ultimately we plan to produce a catalogue of images of estimated dust temperature and column density for these objects. In this paper we briefly discuss the method to be applied in the creation of the images, and present some preliminary results. The latter include the identification of 65 bright southern far-IR regions and estimates of temperature and column density towards their centres.

2 Analysis

2.1 DETERMINATION OF THE TEMPERATURE AND COLUMN DENSITY

Given a gas column density $N(H_2)$ cm^{-2}, the dust temperature T_{dust} and the wavelength dependence of the dust opacity, the brightness measured by *IRAS* can be computed. At wavelengths shorter than about 10 μm a λ^{-1} relationship is generally assumed (e.g. Gatley *et al.* 1977; Harvey, Campbell & Hoffman 1979; Draine & Lee 1984), while a λ^{-2} dependence appears to prevail above 150 μm (e.g. Schwartz 1982; Draine & Lee 1984; Chini, Krugel & Kreysa 1986). The situation between 60 and 100 μm is more uncertain (e.g. Draine & Lee 1984).

In view of the uncertainty we have adopted a λ^{-1} relationship. For a gas-to-dust ratio of 80, the optical depth of the dust τ is given by

$$\tau = 0.5 \times N(H_2) \times 10^{-21}/\lambda, \quad (1)$$

where λ is in micrometres. This formula is only approximate; more precise evaluation using a ratio of 100 (see e.g. Savage & Jenkins 1972) would result in a 22 per cent increase in the computed values.

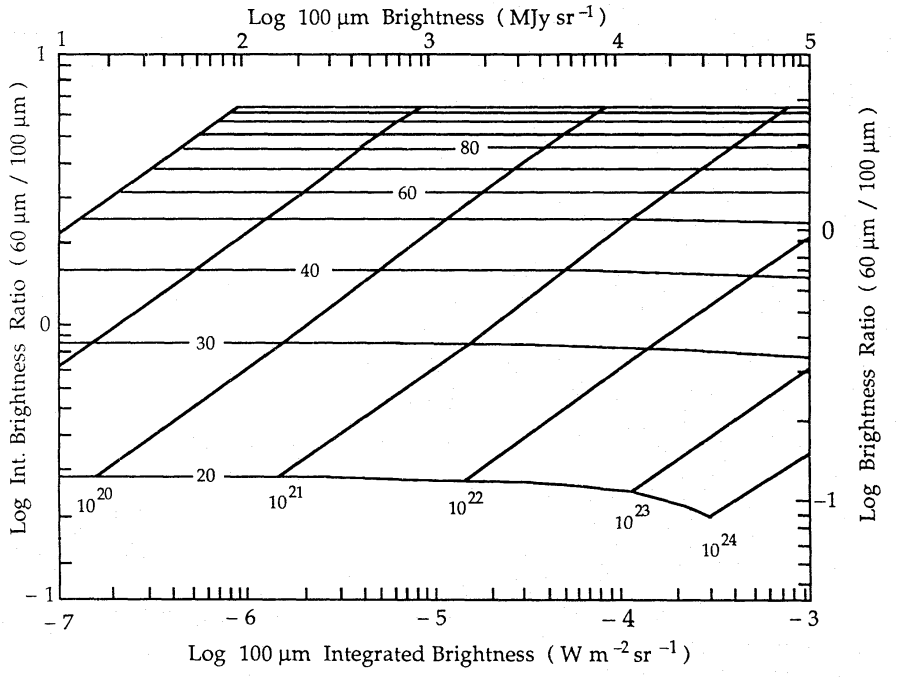

Figure 1. The variation of the ratio of 60 to 100 μm brightness and integrated brightness with 100 μm brightness and integrated brightness, for different values of dust temperature and gas column density.

The brightness is given by

$$\text{brightness}=B_\lambda(T_{\text{dust}})\times[1-\exp(-\tau)], \tag{2}$$

where B_λ is the blackbody wavelength spectrum. This brightness can be integrated over the bandpasses of the *IRAS* detectors (Beichman *et al.* 1985, *IRAS Explanatory Supplement*, Table II.C.5). Fig. 1 shows the calculated ratio of 60–100 μm brightness and integrated brightness plotted against the 100 μm values for a range of temperatures and column densities typical of molecular clouds.

Using a Newton-Raphson iteration, we can invert the above equations to determine the dust temperature and gas column density. The number of iterations required can be greatly reduced if the initial estimates of T_{dust} and τ are close to the correct value. Fig. 1 suggests that, to a good approximation, T_{dust} is a linear function of the ratio, R, of the 60–100 μm integrated brightness. For integrated brightness expressed in W m^{-2} sr^{-1}, T_{dust} can be approximated to within 1 per cent by

$$T_1=19.0+13\times R \tag{3a}$$

for $30<T_1<75$ K. If $R<0.9$, one can extend the 1 per cent validity down to 20 K by

$$T_2=T_1-4.8\times(1-R)^2. \tag{3b}$$

If $R<0.3$, the 1 per cent validity can be further extended down to 15 K by

$$T_3=T_2-[3.1-R\times(19-30\times R)]. \tag{3c}$$

Noting that lines of constant column density in Fig. 1 are nearly straight with a slope of about 0.5, we can produce corresponding equations for the calculation of column density (N cm^{-2}), namely,

$$N_1=4.6\times10^{25}\times F_{100}/R^{1.95}, \tag{4a}$$

where F_{100} is the 100 μm integrated brightness in W m^{-2} sr^{-1},

$$N_2=N_1\times[1+0.52\times(1-R)^2], \tag{4b}$$

and

$$N_3=N_2\times[1.64-R\times(4.2-7\times R)]. \tag{4c}$$

We used T_3 and N_3 as initial estimates for the Newton–Raphson method.

2.2 CORES OF PROMINENT SOUTHERN DUST CLOUDS

The 100 μm maps of the *IRAS* Sky Brightness Images (as described in the *IRAS Explanatory Supplement*, 1985) were used for the identification of the southern dust concentrations. The positions of peak brightness were estimated on maps of the HCON1 and HCON3 series (Hours Confirmation 1 and 3 – the first and third occasions that *IRAS* scanned this region). To allow for differences in the angular resolution of the 60 and 100 μm maps, we derived the average brightness for a 3×3 pixel grid centred on the pixel with the highest brightness. Since the pixel spacing is 2 arcmin, and the basic resolution of the maps is 4–5 arcmin, the brightness would represent an average for a region of size about 8 arcmin. The associated mean background levels around each object were also estimated. By means of the method discussed earlier, these results were then converted into temperatures and column densities.

Table 1 lists the results for the brightest 100 μm regions with declinations south of $-10°$. Because of its complexity the extended dense region near the Galactic Centre has been excluded.

Table 1. Far-infrared properties of southern dust clouds.

Position (1950) R.A.	Dec.	HII region number	Other name	Brightness 100 μm Peak	100 μm B'gd	60 μm Peak	60 μm B'gd	With background T	With background N	Background subtracted T	Background subtracted N	Background T	Background N
h m s	° ′			(10^9 Jy sr^{-1})				K	10^{21}cm^{-2}	K	10^{21}cm^{-2}	K	10^{21}cm^{-2}
08 57 38	−43 33.7	265.15+1.45	RCW36	5.76	0.14	5.80	0.03	49	0.50	49	0.47	24	0.28
08 57 24	−47 19.4	267.94–1.03	RCW38	13.0	0.18	11.1	0.05	45	1.5	45	1.5	27	0.20
09 00 10	−47 32.5	268.45–0.85		3.85	0.18	3.43	0.05	46	0.42	46	0.38	27	0.20
09 01 49	−48 15.3	269.13–1.14		2.04	0.25	1.39	0.06	39	0.37	41	0.28	25	0.39
09 00 34	−48 30.7	269.21–1.45		2.65	0.25	1.69	0.08	38	0.55	39	0.45	28	0.21
09 22 46	−51 46.9	274.01–1.14	RCW42	4.01	0.08	4.24	0.03	50	0.31	51	0.30	30	0.05
10 22 22	−57 31.4	284.31–0.33	RCW49	9.59	0.65	9.56	0.26	49	0.84	50	0.72	31	0.35
10 29 37	−57 46.8	285.25–0.05		5.01	0.40	4.03	0.11	43	0.66	44	0.55	26	0.47
10 41 23	−59 19.5	297.39–0.63	RCW53	11.1	0.50	10.6	0.20	47	1.1	48	0.96	31	0.27
10 42 54	−59 23.7	287.55–0.62	RCW53	5.63	0.50	8.85	0.20	66	0.20	70	0.16	31	0.27
10 44 03	−59 31.2		RCW53	4.73	0.50	3.71	0.20	42	0.66	44	0.53	31	0.27
10 43 50	−59 41.0		RCW53	3.05	0.50	2.35	0.20	42	0.44	44	0.31	31	0.27
10 43 54	−59 56.3		RCW53	2.90	0.50	1.84	0.20	38	0.61	40	0.44	31	0.27
10 45 12	−59 47.2	287.96–0.82	RCW53	2.51	0.50	1.94	0.20	42	0.36	45	0.23	31	0.27
11 09 43	−61 03.0	291.28–0.71	RCW57	10.2	0.40	8.70	0.14	44	1.2	45	1.1	29	0.28
11 12 45	−60 55.8	291.61–0.52		10.6	0.49	13.2	0.20	56	0.61	57	0.55	31	0.25
11 12 58	−61 01.7	291.61–0.52		9.39	0.49	10.9	0.20	53	0.61	55	0.54	31	0.25
12 07 24	−62 33.5	298.23–0.33		4.13	0.31	4.51	0.13	51	0.30	53	0.26	31	0.15
12 12 45	−62 45.4	298.87–0.43		4.37	0.32	3.51	0.18	43	0.58	44	0.52	36	0.09
13 08 07	−62 30.9	305.20+0.02	RCW74	7.57	1.00	6.00	0.28	43	1.0	45	0.75	27	1.1
13 08 11	−62 17.7	305.25+0.20		9.54	1.00	7.69	0.28	43	1.3	45	0.98	27	1.1
13 09 19	−62 19.4	305.36+0.18		9.87	1.00	8.73	0.28	45	1.1	47	0.85	27	1.1
13 11 12	−62 29.9	305.55–0.00		5.21	1.00	4.00	0.28	42	0.76	45	0.47	27	1.1
14 41 22	−59 36.8	316.81–0.04		7.61	0.97	4.92	0.31	38	1.5	40	1.2	28	0.82
15 14 43	−56 27.6	322.15+0.61	RCW92	5.86	0.41	3.93	0.09	39	1.1	40	0.94	24	0.77
15 40 52	−53 56.4	326.65+0.59		8.31	1.05	4.66	0.22	36	2.2	37	1.6	24	2.2
15 49 13	−54 27.3	327.31–0.54		13.0	1.20	7.52	0.33	36	3.3	37	2.7	26	1.4
16 08 21	−51 19.6	331.52–0.07		12.1	2.62	7.70	0.60	38	2.6	41	1.5	25	4.5
16 15 51	−50 56.7	332.66–0.61	RCW106	8.54	1.50	5.53	0.44	39	1.7	41	1.1	27	1.5
16 16 22	−50 46.4	332.79–0.56	RCW106	12.3	1.50	6.32	0.44	35	3.9	35	3.1	27	1.5
16 16 33	−50 31.8			19.8	1.50	11.8	0.44	37	4.7	38	4.0	27	1.5
16 17 09	−50 28.8	333.11–0.44		21.8	1.50	11.3	0.44	35	6.8	35	6.0	27	1.5
16 17 41	−50 18.9	333.29–0.37		17.6	1.50	9.59	0.44	35	5.0	36	4.2	27	1.5
16 18 24	−49 58.8	333.61–0.21		17.5	1.50	11.5	0.44	39	3.5	40	2.9	27	1.5
16 36 16	−48 46.2	336.51–1.48	RCW108	5.82	0.74	4.37	0.27	42	0.88	43	0.67	30	0.48
16 30 55	−47 29.5	336.84+0.05		12.3	3.73	7.15	1.30	37	3.1	40	1.6	29	2.6
16 37 30	−47 01.4	337.95–0.48		8.81	1.76	5.67	0.41	38	1.8	41	1.1	25	2.9
16 37 12	−46 18.0	338.45+0.06		11.3	2.26	7.07	0.57	38	2.5	41	1.5	26	3.2
16 53 19	−40 09.7		RCW116	5.21	0.69	2.68	0.17	34	1.7	36	1.2	25	1.0
16 57 07	−40 28.8	345.23+1.04	RCW116	6.12	0.69	3.85	0.17	38	1.3	39	1.0	25	1.0
16 55 50	−40 06.1	345.31+1.47	RCW116	6.62	0.69	4.36	0.17	39	1.3	40	1.0	25	1.0
16 56 07	−40 06.3	345.40+1.41	RCW116	6.80	0.69	4.58	0.17	39	1.3	41	1.0	25	1.0
16 56 12	−39 59.1	345.53+1.50	RCW116	6.70	0.69	3.45	0.17	34	2.1	35	1.7	25	1.0
17 06 00	−41 32.1	345.43–0.94	RCW117	10.1	0.73	5.98	0.15	37	2.4	38	2.1	24	1.6
17 16 32	−38 54.1	348.72–1.03	RCW122	12.1	0.92	8.91	0.28	41	1.9	42	1.6	28	0.87
17 16 40	−35 52.9	351.19+0.71	RCW127	16.2	1.89	11.3	0.36	40	2.8	42	2.1	23	4.9
17 17 13	−35 44.5	351.36+0.67	RCW127	18.7	1.89	16.6	0.36	45	2.1	48	1.6	23	4.9
17 17 24	−35 43.8	351.36+0.67	RCW127	18.8	1.89	14.0	0.36	41	2.9	43	2.2	23	4.9
17 25 56	−36 38.2	351.64–1.26		10.1	1.00	6.61	0.24	39	2.0	40	1.6	25	1.6
17 22 27	−34 17.7	353.14+0.66	RCW131	16.4	1.17	13.0	0.29	43	2.2	44	1.9	25	1.7
17 21 28	−34 07.4	353.21+0.91	RCW131	12.8	1.17	11.1	0.29	45	1.5	47	1.2	25	1.7
17 47 04	−28 52.7	0.56–0.87	RCW142	5.53	1.48	2.71	0.29	34	2.0	37	0.96	23	3.6
17 44 20	−28 22.3	0.65–0.06	SGR B2	22.9	6.92	7.30	1.23	28	20.0	30	9.5	23	21.0
17 45 32	−27 59.7	1.14–0.10		9.13	6.01	2.30	0.90	26	13.0	32	1.3	21	26.0
17 57 32	−24 03.7	5.90–0.42	W28	10.4	1.74	7.33	0.42	40	1.8	43	1.1	25	2.7
18 00 39	−24 22.7	5.97–1.18		6.54	1.01	7.17	0.24	52	0.48	56	0.31	25	1.6
18 06 23	−20 19.1	10.16–0.36	W31	13.3	1.92	8.22	0.36	38	2.9	40	2.0	23	5.1

Table 1–*continued*

Position(1950) R.A.	Dec.	HII region number	Other name	Brightness 100 μm Peak	100 μm B'gd	60 μm Peak	60 μm B'gd	With background T	With background N	Background subtracted T	Background subtracted N	Background T	Background N
h m s	° '			(10^9 Jy sr^{-1})				K	10^{21}cm^{-2}	K	10^{21}cm^{-2}	K	10^{21}cm^{-2}
18 05 58	−20 05.9	10.31–0.15	W31	7.69	1.92	3.70	0.36	33	2.8	36	1.5	23	5.1
18 05 41	−19 52.6	10.45+0.01	W31	5.35	1.92	1.79	0.36	29	4.1	31	1.7	23	5.1
18 07 30	−19 56.3	10.62–0.39	W31	8.47	1.92	4.27	0.36	34	2.8	37	1.6	23	5.1
18 11 18	−17 55.8	12.81–0.19	W33	14.2	2.40	7.73	0.42	36	4.0	38	2.6	22	7.4
18 17 31	−16 12.3	15.03–0.67	M17	18.9	1.33	14.5	0.32	42	2.7	43	2.3	25	2.1
18 17 49	−16 09.0		M17	15.8	1.33	15.5	0.32	48	1.4	50	1.2	25	2.1
18 15 40	−13 43.7	17.02+0.93	RCW165	5.71	1.05	3.85	0.35	39	1.1	42	0.71	29	0.82
18 22 15	−13 16.6	18.16–0.29		6.31	1.68	3.57	0.36	36	1.7	40	0.82	24	3.3

The positions listed in the first two columns of the table are averages of values derived from HCON1 and HCON3 images and where available, from the *IRAS Point Source Catalog* (Joint *IRAS* Science Working Group, 1985) and the *IRAS Small Scale Structures Catalog* (Helou & Walker 1986). Virtually all the objects are centred within 1 arcmin of bright H II regions, and the third column lists the associated regions in the 5 GHz compilation produced by Haynes, Caswell & Simons (1979). The fourth column lists the associated Hα emission regions from Rodgers, Campbell & Whiteoak (1960). In some cases the 60 and 100 μm background levels around the regions are high and somewhat uncertain, and this uncertainly carries over to the brightness estimates. To show the consequences for the derived parameters, temperatures and column densities have been computed both with and without background removal. These parameters were also computed for the background brightnesses, and are listed in the final columns of the table.

2.3 IMAGES OF TEMPERATURE AND COLUMN DENSITY

We intend ultimately to produce images of estimated dust temperature and gas column density for southern molecular clouds by applying the Newton–Raphson method on a pixel-by-pixel basis for co-added grids of 60 and 100 μm *IRAS* data. Maps derived from calibrated reconstructed detector data will be used in preference to Sky Brightness Images for a number of reasons. The data from the entire survey can be combined in the images, providing higher sensitivity and the potential for enhanced spatial resolution. Software is available which can remove scan-to-scan variations due to detector baseline effects and field gradients due to extended background emission. The principal challenge will be to find a satisfactory algorithm for removal of background emission.

Bright discrete regions that can be effectively separated from the superimposed background emission of the galactic plane are being processed with the facilities of the Infrared Processing and Analysis Center (IPAC). Interactive image processing is used to evaluate the effects of background removal and the subjective determination of cloud boundaries. Using the simple formulae of equations (3) and (4) we have produced grey-scale maps of dust temperature and gas column density for the clouds associated with G291.28−0.71 (RCW 57) and G322.15+0.61 (RCW 92). These preliminary results are shown in Plates 1 and 2; the 'background' level in each 60 and 100 μm image was assumed to be the lowest intensity in the image.

3 Discussion

The results listed in Table 1 suggest that, although the background brightness may contribute significantly to the total brightness observed towards a dust cloud, in most cases the derived

values for dust temperature and gas column density for the cloud are not greatly affected by ignoring the background. Correlation plots of cloud values with and without background subtracted show that ignoring the background would lead to systematically lower temperatures and higher column densities. The largest disparities are associated with the clouds towards the Galactic Centre, where the background emission maximizes.

Fig. 2 shows histograms of the derived dust temperatures for the emission from cloud cores (with background subtraction) and for the background emission. For the clouds 90 per cent of the temperatures are between 30 and 50 K – the median value is 42 K, and 70 per cent of the temperatures are within 5 K of this. In view of the large longitude range for the sample the temperatures are surprisingly similar. The results are consistent with the models of Cox *et al.* (1986), in which the 'warm' dust in H II regions has temperatures of 30–40 K. The background temperature appears to be even more uniform, varying only between 20 and 30 K. There is some evidence for a temperature decrease in directions approaching the Galactic Centre. According to

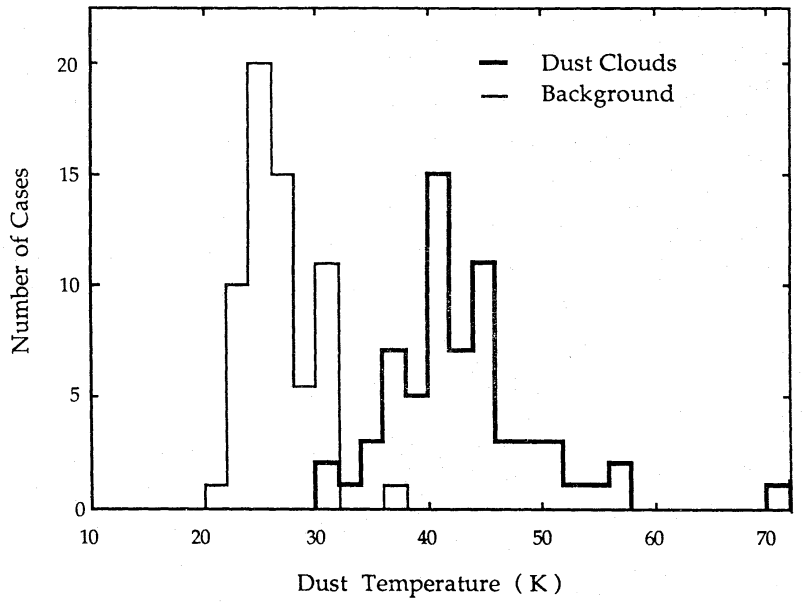

Figure 2. Histograms of the derived dust temperatures for 100 μm regions (with background subtracted) and for the background emission.

Cox *et al.* 'cold' dust with temperatures of 15–25 K is associated with the atomic hydrogen of the galactic disc. Terebey & Fich (1986) have detected a correlation between the hydrogen and infrared 'cirrus'. Although the cirrus temperature derived from the 60 to 100 μm brightness ratio was about 26 K, they argued that the value may be elevated by a contribution from a small population of hotter dust grains.

Although the cloud temperatures are generally similar significant variations occur in some extended clouds. The best example in the present sample is the molecular cloud associated with RCW 53 (the Carina nebula). For G287.55−0.62 the temperature (70 K) is the highest of the sample, and considerably higher than the temperatures (40–48 K) for the other dust peaks in the cloud. This concentration is associated with the nova η Car, a well-known infrared object. Its angular size is considerably less than the angular resolution for the present study, and the true temperature is probably much higher than the listed value.

Fig. 3 shows histograms of column density. The column densities for the dust clouds vary between 2×10^{20} and 10^{22} cm^{-2}; the median value is 1.1×10^{21} cm^{-2}. The maximum density occurs

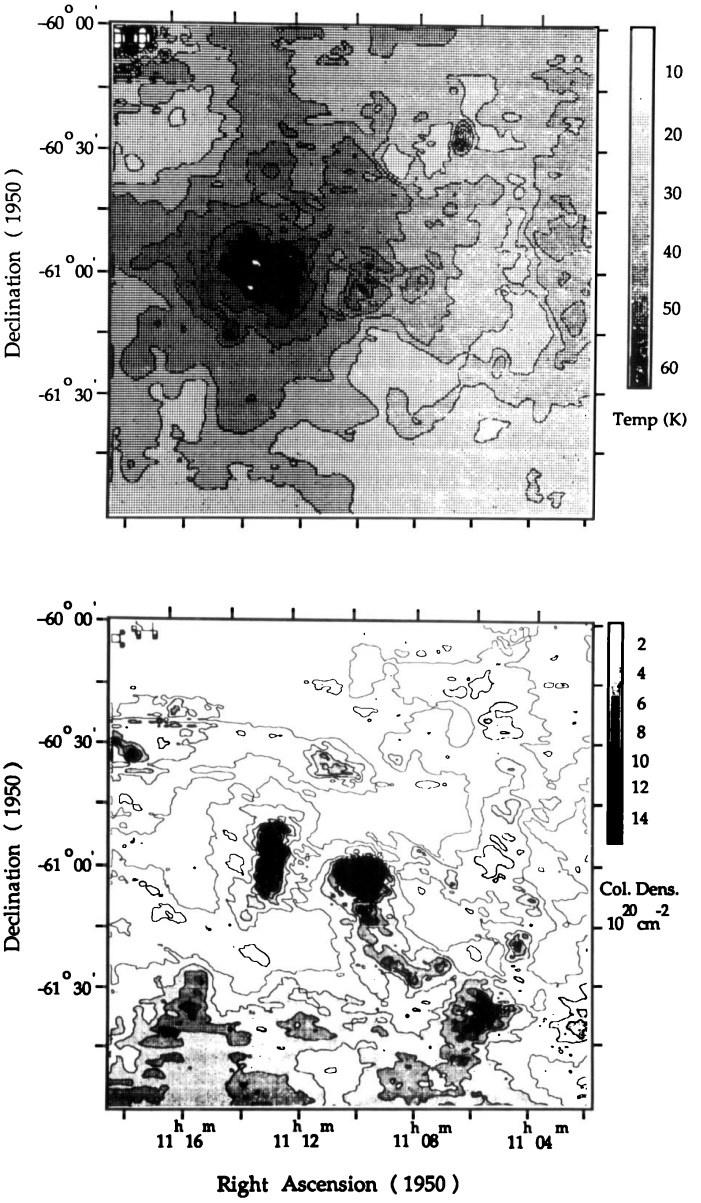

Plate 1. Grey-scale maps of dust temperature and gas column density towards G291.28−0.71 (RCW 57).

[*facing page* 1018]

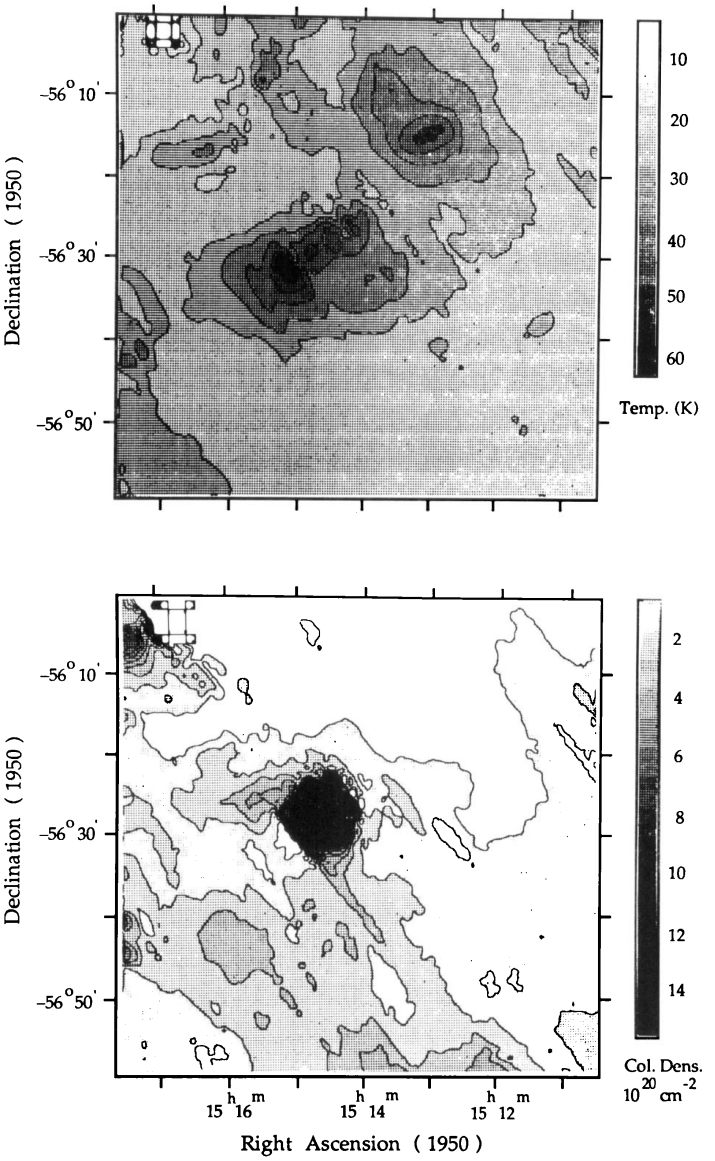

Plate 2. Grey-scale maps of dust temperature and gas column density towards G322.15+0.61 (RCW 92).

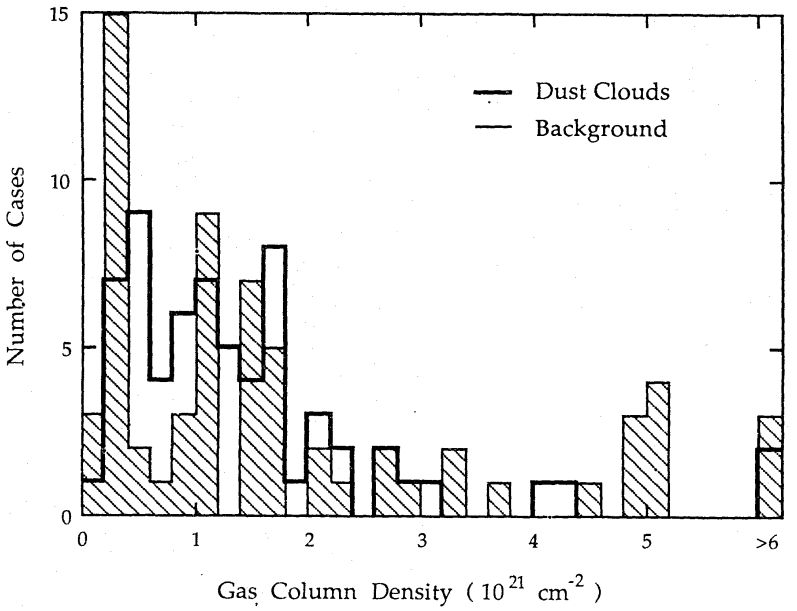

Figure 3. Histograms of the gas column densities for 100μm regions (with background subtracted) and for the background emission. The latter is shown hatched.

for G0.65−0.06 (Sgr B2), the dense H II region-molecular cloud complex near the Galactic Centre. High column densities are also found near galactic longitude 333°. This dust is associated with a well-known group of dense molecular clouds. In fact, the average column density generally increases with longitude, which might be expected when the lines-of-sight begin to include the dense molecular clouds at galactocentric radii of 4–8 kpc (see e.g. Robinson *et al.* 1982). The background densities have a median value similar to the dust clouds. However, they extend to higher values, particularly towards the Galactic Centre region.

An obvious conclusion from the results is that the 60 to 100μm brightness ratio is an excellent indicator of dust temperature and gas column density. Table 1 shows that small changes in temperature are accompanied by large variations in the ratio. Because a λ^{-1} dependence for dust opacity was assumed, whereas the true dependence may be closer to λ^{-2}, the listed temperatures may be systematically high, and the densities low. For example, for a λ^{-2} dependence the median temperatures for the dust clouds and background would be reduced by about 6 and 2 K, respectively.

The maps in Plates 1 and 2, produced with an angular resolution of about 3 arcmin, show considerably more detail than is supplied by Table 1 for the same objects. Plate 1 contains three dust clouds associated with G291.28−0.71 (RCW 57) and G291.61−0.52. The cooler, denser nature of the former is obvious (it is associated with a prominent southern molecular cloud). Plate 2 shows considerable temperature and density structure for the dust associated with G322.15+0.61 (RCW 92). The extra temperature maximum at the top of the figure, without an associated density concentration, warrants further investigation.

4 Conclusion

The study has shown that southern molecular clouds can be effectively pinpointed using the *IRAS* far-infrared sky survey. A sample of 65 southern objects was selected on the basis of *IRAS* Band 4 (100μm) brightness. These were found to be associated with previously identified southern molecular clouds, and close to H II regions.

The dust temperature and gas column density of most molecular clouds can be conveniently estimated from *IRAS* Band 3 (60 μm) and Band 4 (100 μm) images using simple approximations. For prominent clouds, including extended background emission, the results are quite insensitive to the assumed zero level in the original *IRAS* images. With an angular resolution of around 8 arcmin, temperatures and column densities were derived for the selected cloud sample. The temperatures were remarkably similar – 90 per cent were in the range 37 to 47 K. A similar situation was also found with the background emission, although in a lower temperature range (21–31 K). The gas column densities for the clouds ranged from 2×10^{20} to 10^{22} cm^{-2}, with a median value of 1.1×10^{21} cm^{-2}. These characteristics may apply only to the 'active' regions of molecular clouds, pinpointed by the presence of H II regions, because no cool quiescent clouds were included in the sample. Presumably the latter are of lower brightness, reflecting the different physical conditions within the clouds.

Preliminary maps of temperature and column density, derived using the calibrated reconstructed detector data, indicate that this is a powerful approach for detailed investigation of molecular clouds. Maps of derived column density may turn out more effective than 100 μm brightness maps in highlighting the more interesting (i.e. the denser) molecular clouds.

Acknowledgments

We are grateful to Dr Nick Gautier for assistance in adapting his software to process *IRAS* images in the manner described in this paper. This research was performed in part at the Jet Propulsion Laboratory, California Institute of Technology, under contract with the US National Aeronautics and Space Administration. Part of the reported work was carried out by Gwen Manefield at CSIRO Division of Radiophysics.

References

Beichman, C. A., Neugebauer, G., Habing, H. J., Clegg, P. E. & Chester, T. J., 1985. *IRAS Catalogs and Atlases, Explanatory Supplement,* US Government Printing Office, Washington DC.

Chini, R., Krugel, E. & Kreysa, E., 1986. *Astr. Astrophys.*, **167,** 315.

Cox, P., Krugel, E. & Mezger, P. G., 1986. *Astr. Astrophys.*, **155,** 380.

Draine, B. T. & Lee, H. M., 1984. *Astrophys. J.*, **285,** 89.

Gatley, I., Becklin, E. E., Werner, M. W. & Wynn-Williams, C. G., 1977. *Astrophys. J.*, **216,** 277.

Harvey, P. M., Campbell, M. F. & Hoffman, W. F., 1979. *Astrophys. J.*, **228,** 445.

Haynes, R. F., Caswell, J. L. & Simons, L. W. J., 1979. *Aust. J. Phys. Astrophys. Suppl. No. 48,* 1.

Helou, G. & Walker, D., 1986. *IRAS Small Scale Structures Catalog,* US Government Printing Office, Washington DC.

Joint *IRAS* Science Working Group, 1985. *IRAS Point Source Catalog,* US Government Printing Office, Washington DC.

Robinson, B. J., McCutcheon, W. H., Manchester, R. N. & Whiteoak, J. B., 1983. In: *Surveys of the Southern Galaxy,* p. 1, eds Burton, W. B. & Israel, F., Reidel, Dordrecht, Holland.

Rodgers, A. W., Campbell, C. T. & Whiteoak, J. B., 1960. *Mon. Not. R. Astr. Soc.*, **121,** 103.

Savage, B. D. & Jenkins, E. B., 1972. *Astrophys. J.*, **172,** 491.

Schwartz, P. R., 1982. *Astrophys. J.*, **252,** 589.

Terebey, S. & Fich, M., 1986. *Astrophys. J.*, **309,** L73.

Whiteoak, J. B., 1983. In : *Surveys of the Southern Galaxy,* p. 31, eds Burton, W. B. & Israel, F., Reidel, Dordrecht, Holland.